

Initiation processes for run-off generated debris flows in the Wenchuan earthquake area of China



W. Hu^{a,*}, X.J. Dong^{a,*}, Q. Xu^a, G.H. Wang^c, T.W.J. van Asch^{a,b}, P.Y. Hicher^d

^a State Key Laboratory of Geo-Hazard Prevention and Geo-Environment Protection, Chengdu University of Technology, Chengdu, 650023, People's Republic of China

^b Faculty of Geosciences, Utrecht University, Heidelberglaan 2, 3584, CS, The Netherlands

^c Disaster Prevention Research Institute, Kyoto University, Japan

^d LUNAM University, Ecole Centrale de Nantes, CNRS UMR 6183 GeM, France

ARTICLE INFO

Article history:

Received 24 May 2015

Received in revised form 26 October 2015

Accepted 27 October 2015

Available online 30 October 2015

Keywords:

Run-off

Debris flow

Fluidization

Damming and breaching effect

ABSTRACT

The frequency of huge debris flows greatly increased in the epicenter area of the Wenchuan earthquake. Field investigation revealed that runoff during rainstorm played a major role in generating debris flows on the loose deposits, left by coseismic debris avalanches. However, the mechanisms of these runoff-generated debris flows are not well understood due to the complexity of the initiation processes. To better understand the initiation mechanisms, we simulated and monitored the initiation process in laboratory flume test, with the help of a 3D laser scanner. We found that run-off incision caused an accumulation of material down slope. This failed as shallow slides when saturated, transforming the process into debris in a second stage. After this initial phase, the debris flow volume increased rapidly by a chain of subsequent cascading processes starting with collapses of the side walls, damming and breaching, leading to a rapid widening of the erosion channel. In terms of erosion amount, the subsequent mechanisms were much more important than the initial one. The damming and breaching were found to be the main reasons for the huge magnitude of the debris flows in the post-earthquake area. It was also found that the tested material was susceptible to excess pore pressure and liquefaction in undrained triaxial, which may be a reason for the fluidization in the flume tests.

© 2015 Elsevier B.V. All rights reserved.

1. Introduction

The 2008 Wenchuan Earthquake in the Sichuan Province, China generated many landslides (Fig. 1), which produced a huge amount of loose deposits. These loose deposits have caused a dramatic increase in debris-flow occurrence in subsequent years. The mechanism of these debris flows is only incompletely understood. The mechanism is complex due to the interaction of different processes such as run-off induced gully erosion in initially unsaturated granular deposits, and damming and breaching effects caused by side-wall instability in the gullies.

Debris-flow initiation can be generally subdivided into two mechanisms: 1) failure of shallow landslides, which transform into debris flows, and 2) concentrated run-off (flash flood) erosion in channels filled with sediments which may be supplied by landslides from the slope. Such debris flows contain a small fine fraction (less than 10–20% silt and clay; Tang et al., 2012 compared to soils involved in landslide-induced debris flows, and the source materials have a much higher hydraulic conductivity. Tognacca and Bezzola (1997), Cannon et al. (2003) and Berti and Simoni (2005) studied debris flows initiated by channel-bed mobilization, which is only one of the initiation processes of debris flows confined in channels. A framework that adequately

describes all of the processes involved in the initiation of debris flows is still missing (e.g., Johnson and Rodine, 1984; Cannon et al., 2001; Berti and Simoni, 2005; Larsen et al., 2006; Coe et al., 2008; Gregoretti and Fontana, 2008). Moreover, previous studies focused mainly on sediment erosion. More recently, Kean et al. (2013) concluded that debris-flow initiation by runoff can be grouped into two categories: mass failure of the channel sediment by sliding along a discrete failure plane and grain-by-grain bulking by hydrodynamic forces. The former process requires a sudden large impulse of sediment to be added to and/or entrained within the water flow, such as from the failure of the sediment-filled bed of the channel or failure of channel banks. The latter process has been observed in some sediment transport experiments in steep flumes (e.g., Tognacca et al., 2000; Gregoretti, 2000; Armanini et al., 2005). In some of these experiments, a debris-flow surge is produced by hydrodynamic forces eroding individual particles at the surface rather than by sliding along a failure plane at a certain depth. There are, however, other mechanisms involved in the initiation process.

Several huge erosion gullies were found after debris flows occurred in the Wenchuan earthquake area in southwest of China. The aim of this paper is to explore the interacting processes involved in the generation of these erosion gullies related to debris flows. For this purpose, a series of flume tests simulating erosion and incision by run-off water were conducted. By using a laser-scanning technique, a sequence of

* Corresponding author.

E-mail address: 16704937@qq.com (X.J. Dong).

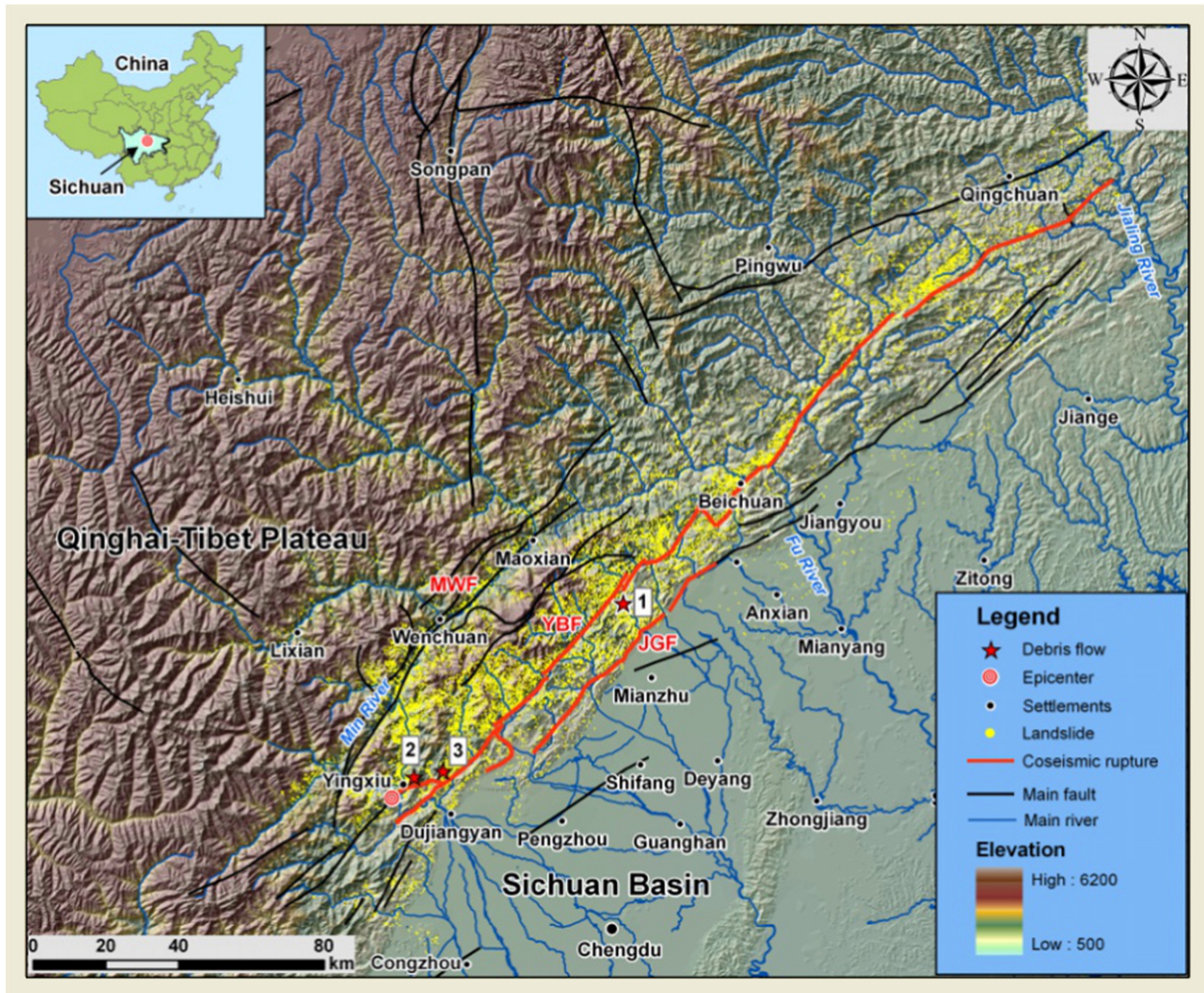


Fig. 1. Distribution map of landslides triggered by the Wenchuan Earthquake and three catastrophic debris flows triggered by the rainstorms on 13 August 2010. (MWF: Maoxian-Wenchuan Fault; YBF: Yingxiu-Beichuan Fault; JGF: Jianguo-Guanxian Fault. 1: Wenjia gully and Zoomaling gully debris flows near Qingping Town; 2: Hongchun gully debris flow; 3: Longchi debris flow). The landslide distribution map was derived from a rapid landslide inventory made by Huang and Li (2009).

processes related to the initiation of debris flows was monitored to understand which processes played a major role in the initiation and enlargement of the erosion gully.

2. Post-earthquake debris flows in SW China

At least 72 debris flows were induced in Beichuan County close to the Wenchuan earthquake epicenter, due to a major rainfall event on the 24th of September 2008, causing 42 casualties (Tang et al., 2009). In addition, a heavy rainstorm on the 13th–14th of August 2010 near the town of Yingxiu, located at the epicenter of the Wenchuan earthquake, triggered many landslides and channelized debris flows. Three catastrophic debris flows were positioned in Fig. 1. On the 13th of August 2010 numerous debris flows occurred along the Qingping section of the Mianyu River, (Tang et al., 2012; Xu et al., 2012). The Wenjia gully debris flow located in the Qingping section of the Mianyu River was the largest among these debris flows. The loose source material of this debris flow was deposited by a rock avalanche due to the Wenchuan earthquake. The high energy of the rock avalanche was able to entrain the shallow, loose, soil material along its flow path; therefore, the deposited material has a volume of $>7.0 \times 10^7 \text{ m}^3$. On the 13th of August 2010, heavy rain generated intensive runoff that produced the debris flow and a huge erosion channel. Fig. 2a gives an overview of this erosion channel. Fig. 2b,c shows the erosion channel with a depth of 40–60 m and a width of 50–100 m.

Fig. 2d shows a widening of the erosion channel, caused by slope failures during the incision of the channels. Fig. 2e shows the photograph of the location so-called “1300 platform” that supplies loose material for debris flows.

From the photographs in Fig. 2, we concluded that the incision of the material was caused by gully erosion. The widening of the gully was caused by slope instability as shown by the shape of the slope formed by slumping (see Fig. 2b–d). However these photographs do not give a complete insight into the sequence of processes leading to the initiation of the debris flows and the formation of the huge erosion gully. We used flume tests to simulate the whole initiation process and special attention was given to studying gully formation.

3. Experimental set-up and test procedures

The flume was instrumented in order to obtain the hydrological changes and the deformation of the deposits during the initiation process. The equipment is described in Hu et al. (2015). The materials for the flume tests were collected at the top of the 1300 platform in the Wenjia gully (Fig. 2a), which was the source of loose material for the debris flow. There are differences in grain-size distributions between the in situ materials taken from different locations. An average grading is presented in Fig. 3. The largest particle in the average grading is 100 mm. In order to avoid boundary effects we chose a similar grading, but 10 times smaller than the grading of the in situ material

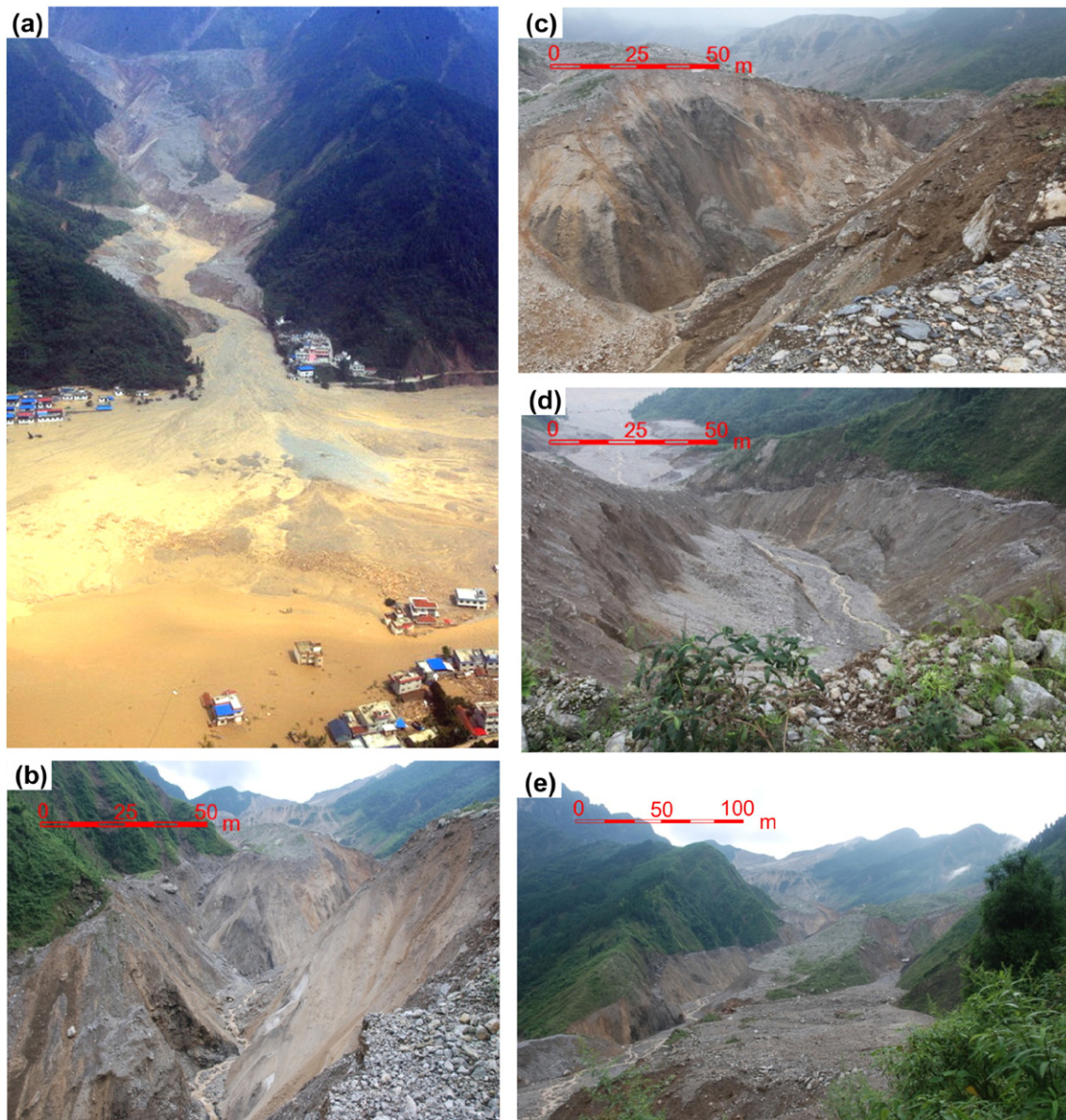


Fig. 2. Photos of the 8.13 Wenjia gully debris flow. (a) overview; (b) and (c) source area with deep channel erosion. (d) channel widening; (e) channel erosion (Xu et al., 2012).

as shown in Fig. 3. The tested material consists of sub-angular limestone particles (ASTM D2488-93, 2009).

In order to prepare soil samples with homogenous initial moisture content, the particles were dried and sieved and mixed with fines. Then an amount of water was supplied according to the desired initial water content. The soil was carefully mixed with the water to ensure soil homogeneity. Then a film was used to cover and seal the samples. The soil was then covered, sealed and stored for 24 h prior to the construction of the model. The initial moisture content was about 1.5% for all the tests.

The soil was compacted layer by layer with a thickness of 10 cm in order to build a soil model with nearly the same initial void ratio. The average initial void ratio for the sample was 0.43 and the relative density is 45% with maximum void ratio (e_{\max}) being equals to 0.561 and minimum void ratio (e_{\min}) 0.29. The runoff was simulated by a concentrated water flow supplied by a pump, and the water outlet was 25 cm above the surface positioned at the back of the model (Hu et al., 2015). Discharge was accurately controlled by a flow meter and a flow valve. The washed-out materials were collected every 20 s, dried and sieved to determine the grain size distributions and quantify the amount of erosion.

4. Test results and interpretation

About 10 tests were carried out with different slopes varying from 12° to 35°, which provoked the same initiation process. Tests with a slope of 28° were selected for the presentation of this process. Two tests were carried out with the same initial conditions of a 28° slope and a runoff discharge of $0.0003 \text{ m}^3 \text{ s}^{-1}$. One test was stopped several times for 3D scanning of the erosion channels. Another one was carried out without any pause to obtain the erosion curve during the initiation of the debris flow. Study of the videos of these two tests showed that the pauses did not appear to change the initiation mechanism nor the process.

The 3D scanner results are shown in Fig. 4. The development process of the debris flow could be divided into six stages.

Stage I: A small gully was formed at the top of the slope due to runoff surface erosion. The eroded particles were deposited in the lower part, as shown in Fig. 4a, due to the decrease of the seepage force. Most of the run-off water infiltrated into this slope deposit, decreasing the runoff depth and consequently shear force of the remaining runoff which consequently entrained smaller particles. At this stage, no debris flow was initiated (Fig. 4a).

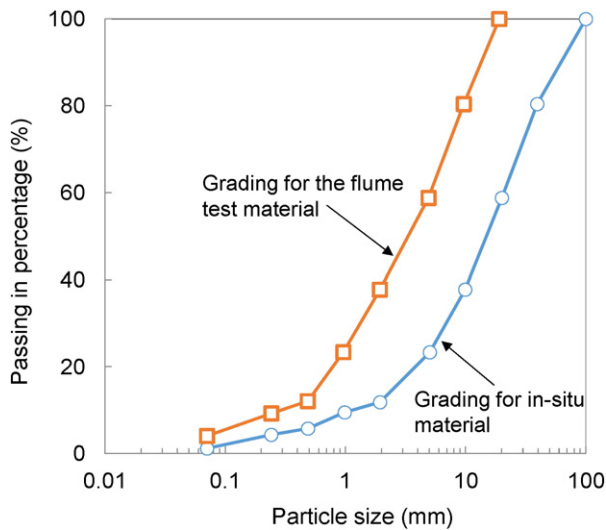


Fig. 3. Grain size distributions of in-situ material and material used in the flume.

Stage II: The water continued to infiltrate into the slope deposits. The finest particles were washed out due to the seepage force of the infiltrated water. According to a laser particle-size analyzer, these particles were smaller than 0.05 mm. The washing out of the fine particles decreased the density and hence the shear strength of the deposited material and made the material more sensitive to static liquefaction. After about 5 min from the beginning of the test, a complete fluidization of the deposited soil mass occurred and the mass transformed into a debris flow. A gully formed at the toe of the slope due to this fluidization process, as shown in Fig. 4b.

Stage III: The erosion gully continued to deepen and widen due to sediment erosion and entrainment (Fig. 4c).

Stage IV: As a result of continued water infiltration into the soil, the sides of the erosion gully became unstable and small landslides initiated, which dammed the gully with debris (Fig. 4d).

Stage V: There was a quick rise of water level behind the landslide dam, which became saturated. After about 20 s, the dam breached by a combination of overtopping and internal erosion. The debris from the breached landslide dam formed a larger debris flow. This damming and breaching process greatly increased the volume of the debris flow and widened and deepened the erosion gully as shown in Fig. 4e.

Stage VI: The process of damming and breaching continued and enlarged the erosion gully. Sediment erosion also played a role, but much less than the damming and breaching. A large erosion channel was created, as shown in Fig. 4f.

By comparing the digital maps at different erosion stages with the initial slope topography, an isopath map for the different stages was obtained (Fig. 5). The change in topography from Fig. 5a–b was caused by the shallow landslide of the deposited material at the toe of the slope. From Fig. 5b–c, the topographic change was caused mainly by bed and side erosion. From Fig. 5d–e, it was caused by breaching of the dammed materials. From Fig. 5e–f, it was caused mainly by episodic damming and breaching and partly by bed erosion.

Two positions of representative cross sections at the upper and lower parts of the slope were selected to show the change of the profiles at the different stages (Fig. 6). The change from initial profile to Profile 1 (Fig. 6) was caused by the superficial erosion (upper section) and deposition (lower section). Profiles 2 and 3 show the effect of bed and lateral erosion. Profiles 3 and 4 of the lower cross section show the damming of the gully caused by the instability of the two banks. Profiles 4 and 5 depict the dam breaching by overtopping and the large widening and deepening of the gully in both upper and lower parts. Profiles 5 and 6 show the enlargement of the gully mainly caused by the damming

and breaching as observed in the video. When we compare the successive profiles, it became clear that damming and breaching contributed much more to the enlargement of the erosion gully than did the bed erosion and the initial shallow landslide.

A second similar test was carried out without interruption for scanning to measure the erosion during the test. The amount of erosion each 20 s and the cumulative erosion are shown in Fig. 7. In Fig. 7a, the first peak was caused by the fluidization of the deposits at the foot of the slope. It can be considered as the initiation of the debris flow. The video recording showed that the time of the dam breaching generated by the instability of the banks corresponded to the next peaks in Fig. 7a. In Fig. 7b, the steps in the curves were all caused by damming and breaching after the initiation of the debris flow.

The above observations show that damming, breaching and fluidization of the loose deposits generated peaks in the concentration of transported sediments and played key roles in the initiation and development of the debris flows.

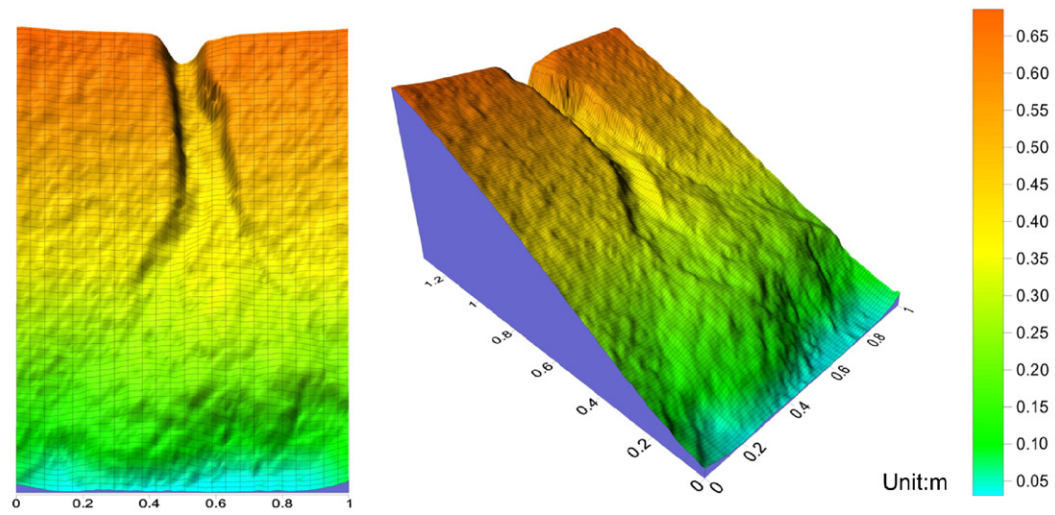
5. Fluidization mechanism

As discussed in Section 4, fluidization of the loose deposits was important in the initiation of a debris flow. In addition, the mechanism for the breaching of the dammed material was not very clear. Video observations showed that overtopping was obviously an important mechanism. However, it was difficult to consider that overtopping solely could cause such a sudden increase of width and height of the erosion gully after the breaching of the dammed material. Fluidization of the bottom part of the dammed material was a possible explanation for this phenomenon.

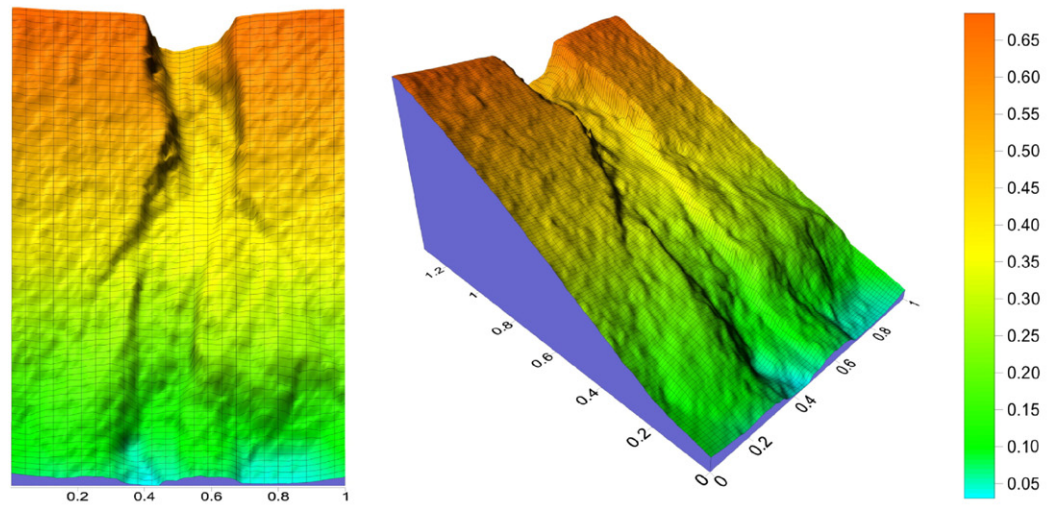
Liquefaction is a possible mechanism of the fluidization. Liquefaction could lead to instabilities in large masses of soil, commonly referred to as flow slides (Kramer and Seed, 1998; Hird and Hassona, 1990; Eckersley, 1990; Ishihara, 1993; Darve, 1996; Daouadji et al., 2010). Static liquefaction was a possible reason for the fluidization (Olivares, 2001).

As shown in Fig. 8, the pore pressure recorded from the bottom of the flume gave more support to the liquefaction hypothesis. The pore pressures along the base increased slowly, with a sharp transient at the fluidization of the deposited material which corresponded to stage II in Section 4. Very significant excess pore pressures were generated during the failure of the deposited material. Fig. 8b shows detail of the sharp increase in pore pressure. It only lasted about 2 s and suddenly decreased the effective stress at the bottom of the soil. The sensor No. 1 recorded the highest excess pore pressure, 2.4 kPa (1 kPa roughly equals to 10 cm of water).

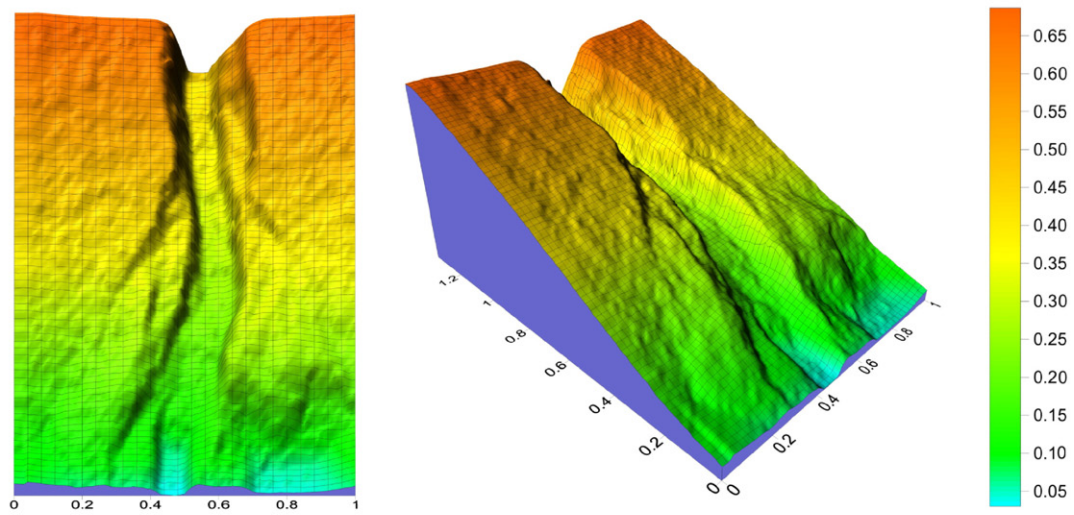
The liquefaction potential of the flume material was also evaluated using undrained triaxial tests. The samples were compacted to have the same density as the average density of the flume materials. The samples were all fully saturated. The tests results were shown in Figs. 9 and 10. The samples were consolidated to four different minor principal effective stresses (30, 50, 100 and 150 kPa). The sample under 150 kPa exhibited dilative behavior with decreasing excess pore-water pressure and increasing deviator stress at high strains. The sample under 100 kPa initially appeared to liquefy, straining rapidly to about 13% but then began to dilate a little at higher strains, as shown in Figs. 9b and 10. This type of behavior was first observed and described as “limited liquefaction” by Castro (1969). The samples tested under 50 and 30 kPa were both liquefied. After peak deviator stress was reached, both excess pore water pressure and the rate of straining increased rapidly as the samples strained at residual deviator stress less than the peak deviator stress. The instability line (Lade et al., 1998) changed with the change of cell pressure. The slope of it decreased with the decrease of cell pressure, indicating that the instability resistance decreased with increase of cell pressure. These tests revealed that the tested material is very easy to liquefy under pressures, even smaller than about 50 kPa.



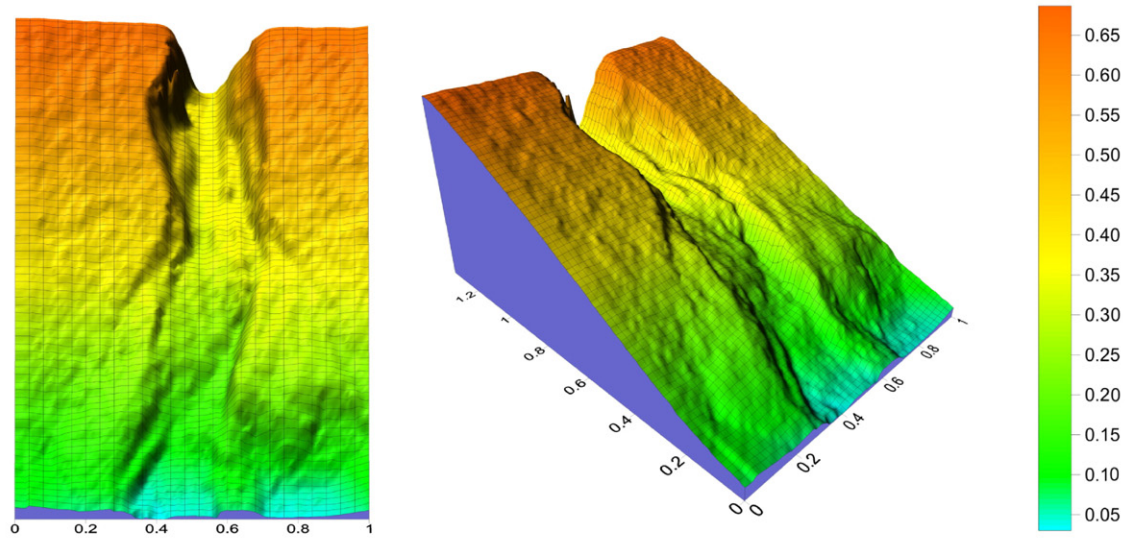
(a) Stage I



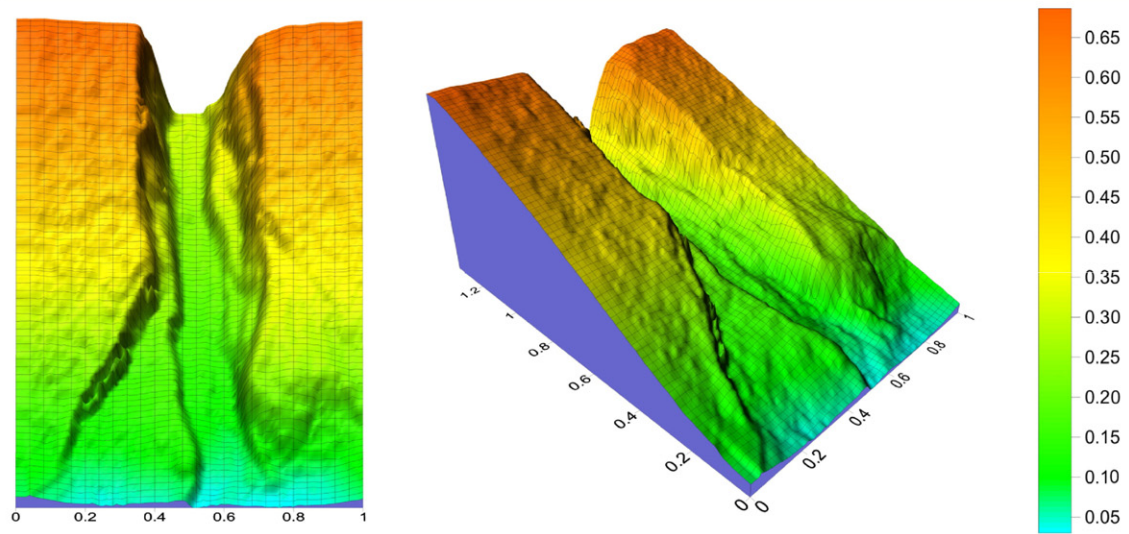
(b) Stage II



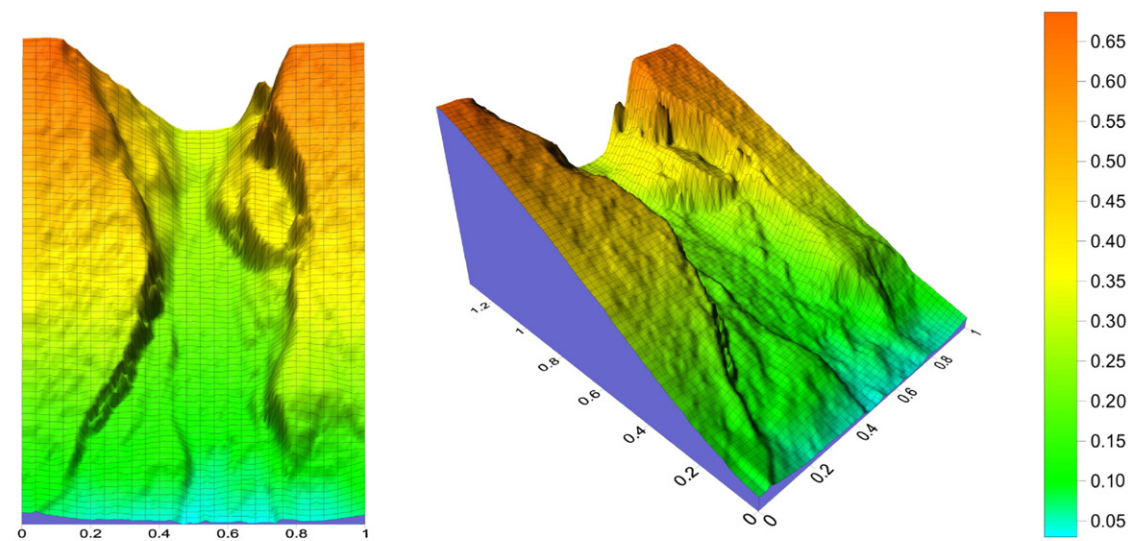
(c) Stage III



(d) Stage IV



(e) Stage V



(f) Stage VI

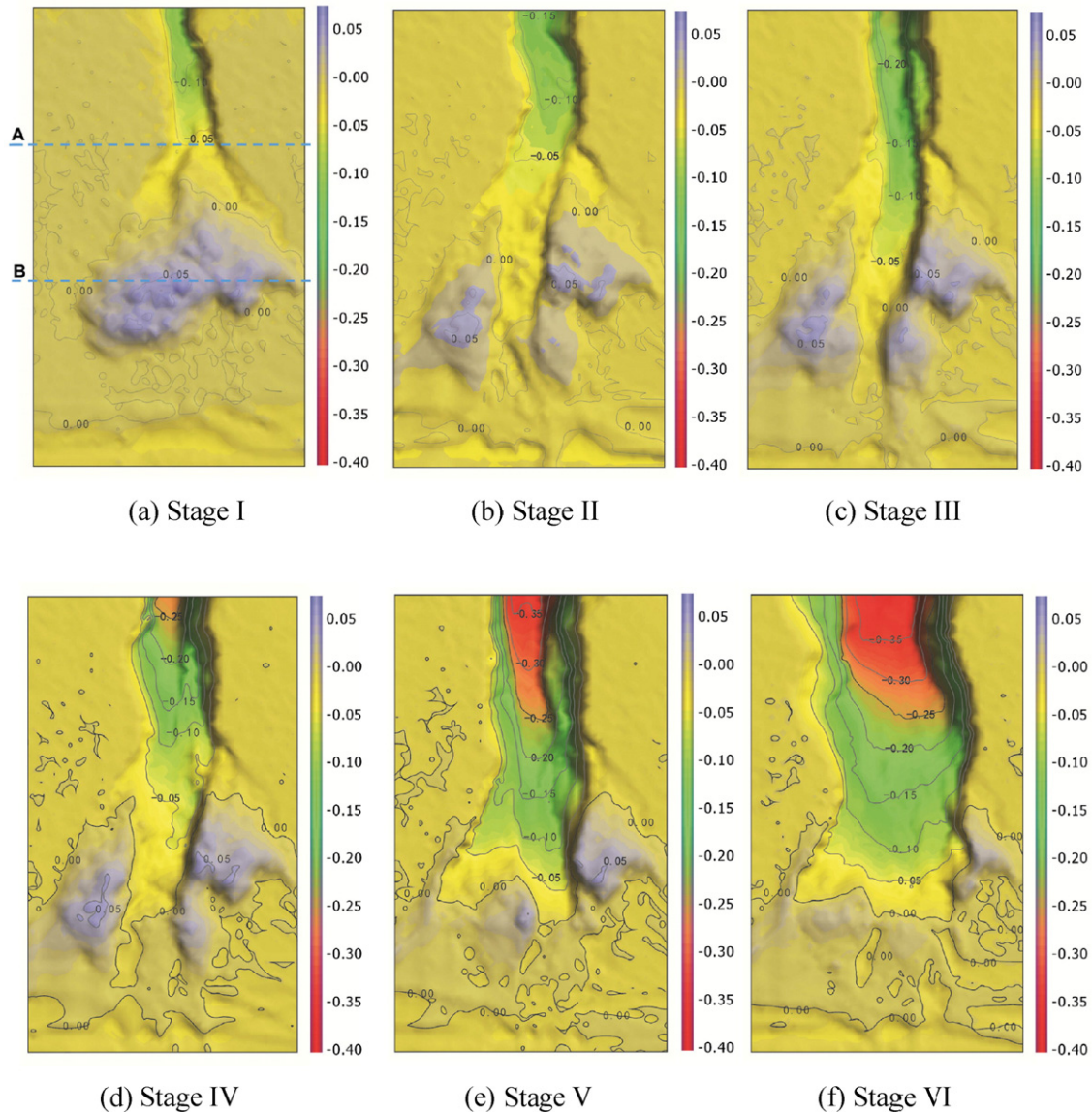


Fig. 5. Isopath maps for different stages of a debris flow. Positive contour numbers indicate deposition and negative numbers indicate erosion with respect to the initial slope surface (in m).

6. Discussion and conclusions

Many huge debris flows were initiated after the 12 May 2008 Wenchuan earthquake in southwestern China. With the help of flume tests and a 3D laser scanner, we monitored a sequence of processes leading to the development of debris flows. Superficial run-off erosion first created a small erosion gully in the upper part of the slope and the eroded material was deposited in the lower part. The debris flow process initiated through saturation and breaching of this deposited material, which blocked the run-off water. Bed erosion and lateral erosion then continued to enlarge the erosion gully providing future material to the debris flow at lower concentrations. The subsequent erosion peaks with high debris-flow solid concentrations, were related to the cyclic damming by side-wall failures and dam breaching which enlarged the erosion gully and the size of the debris flow. These cyclic processes provided one of the explanations for the surging character

often seen in debris flows in the field (e.g. [Coe et al., 2008](#); [Kean et al., 2013](#)).

A question arises whether the experiments mimicked exactly the real in-situ processes and whether the scale of the laboratory test influenced its outcome of the compared to the field results. We believed that our experiments simulated a sequence of essential processes which explained the morphological evolution of the source deposits and the generation of the debris flows. The scale may affect the quantitative output but not the type, sequence and mechanism of the processes. Similar to the experiments, a study of the Wenjia gully ([Tang et al., 2012](#)) showed that, in the course of the years after the Wenchuan earthquake an incision was followed by a widening of the gully and production of five debris flows.

The continual damming and breaching highlighted by our experiments showed the complexity of the processes related to the supply of material for the initiation and development of debris flows and the

Fig. 4. Digital elevation models (DEMs) showing topographic changes. (a) Stage I: surface erosion and deposition of loose material. (b). Stage II: shallow landslide in the deposited materials and initiation of debris flow. (c) Stage III: channel bed erosion. (d). Stage IV: instability of the side wall of the erosion channel and damming. (e). Stage V: breaching of the dammed material and enlargement of the channel. (f). Stage VI: Continual breaching and damming and enlargement of the channel. The thickness of the soil is symbolled by different colors with the unit of meter.

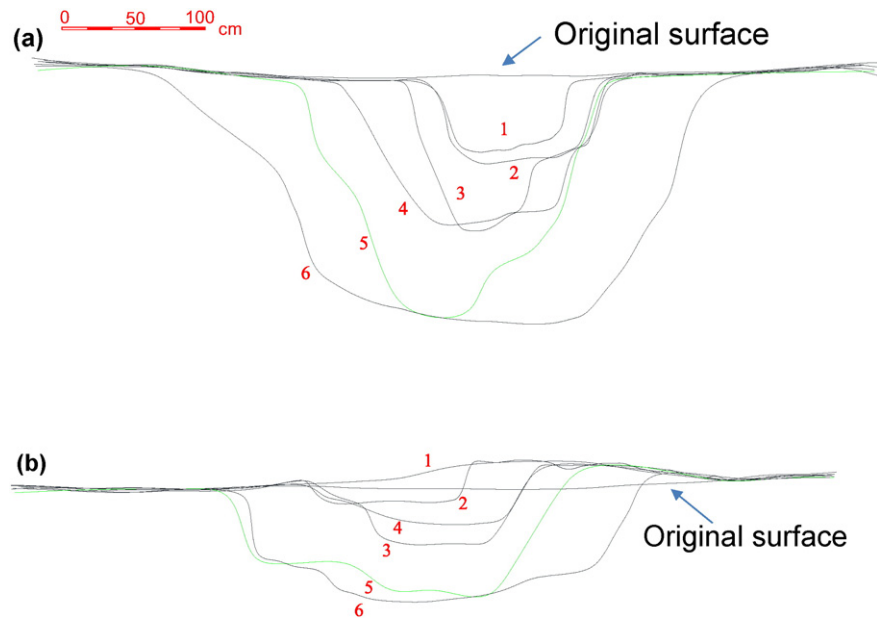


Fig. 6. Cross sections of the erosion channel at different stages. Numbers 1 to 6 correspond to the cross sections from stages I to VI. (a) and (b) are respectively corresponding to sections A and B in Fig. 5.

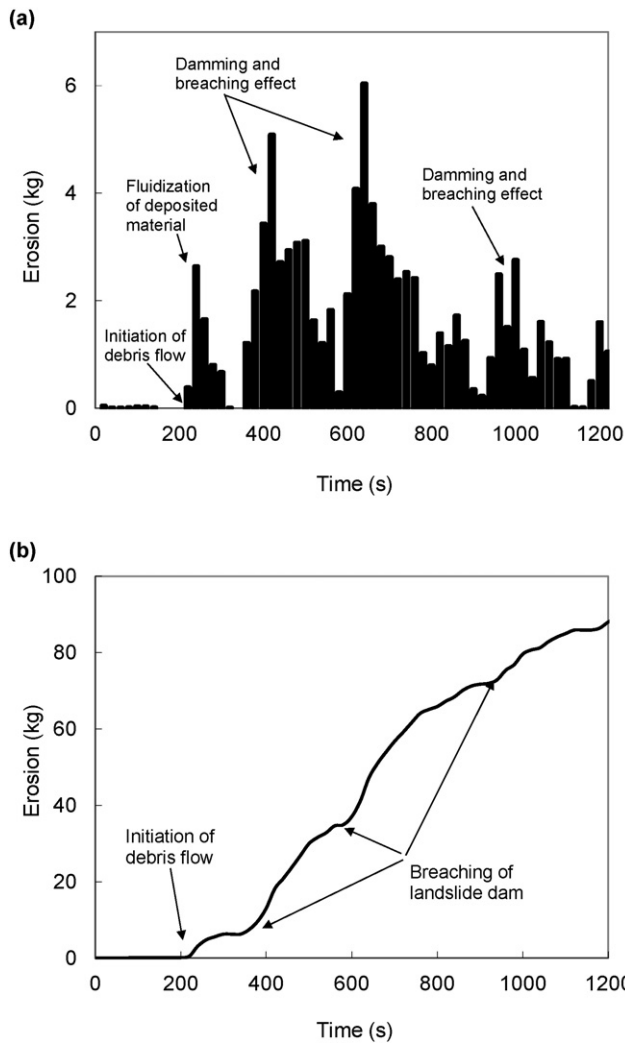


Fig. 7. Erosion amount during the debris flow development. (a) Erosion rate at 20 s intervals. (b) Cumulative erosion curve.

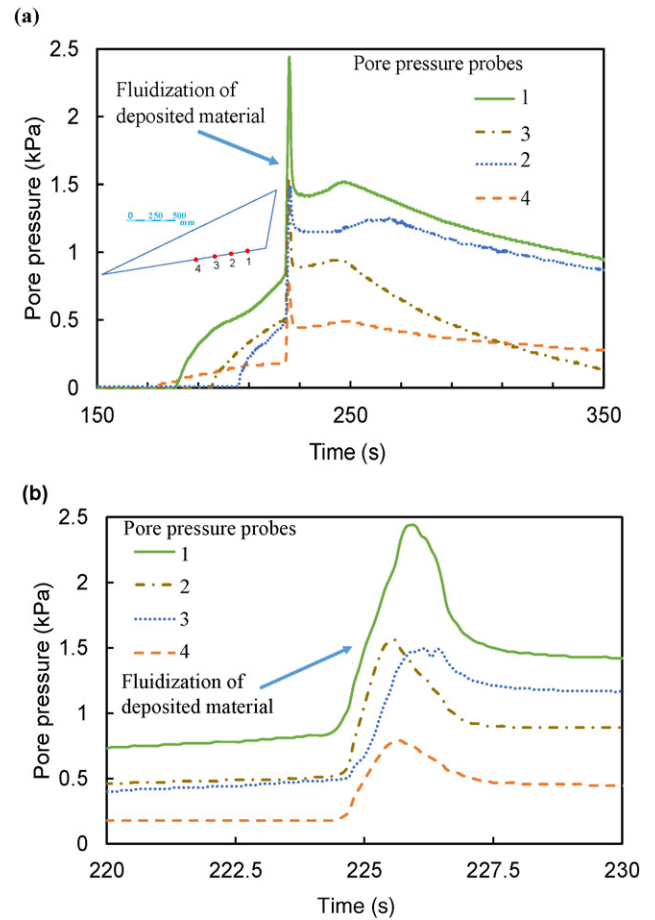


Fig. 8. Evolution of pore pressure during the fluidization of the deposited material at stage II. (a) 150 to 350 s. (b) 220 to 230 s. The triangle is the outline of the model. The red points are the symbols of the pore pressure sensor, which are located at the bottom of the flume.

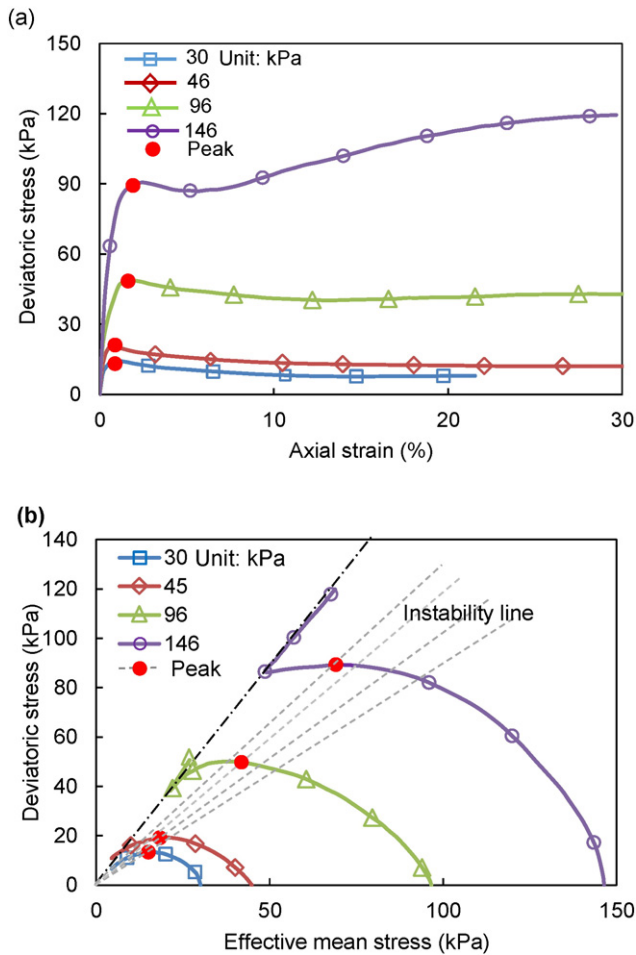


Fig. 9. Undrained triaxial test results for the flume material. The instability line was determined by connecting the point (0, 0) with the undrained curve vertex.

big challenge to model these processes. The chain of processes showed by the flume tests with runoff erosion (lateral erosion and incision), slope failure, damming and breaching, and bed failure (not simulated in our experiments) is usually simplified by equations considering only a part of these processes (e.g., Tognacca et al., 2000; Berti and Simoni, 2005; Iverson et al., 2011; Cui et al., 2013; Kean et al., 2013) or by approximating the material supply to debris flow using erosion

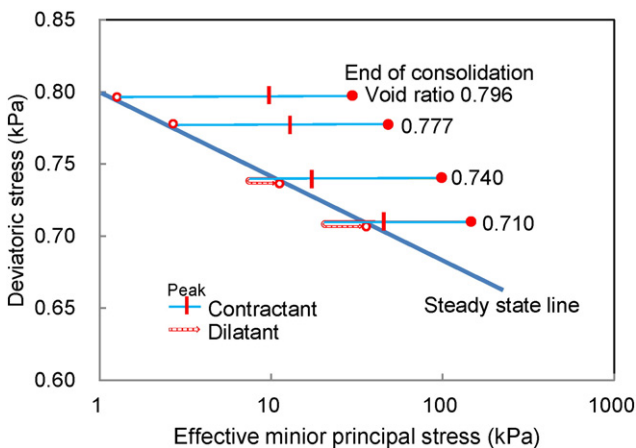


Fig. 10. Steady state line of the sample determined from undrained tests of the flume material.

rates related to flow velocity and flow depth (Eglit and Demidov, 2005; McDougall and Hungr, 2005; Van Asch et al., 2014).

Acknowledgements

This research was financially supported by the National Basic Research Program of China: National fundamental scientific research grant (No. 41472273); and the Public Welfare Project from the Ministry of Land and Resources of People's Republic of China (2013-11122).

References

- Armanini, A., Capart, H., Fraccarollo, L., Larcher, M., 2005. Rheological stratification of liquid-granular debris flows down loose slopes. *J. Fluid Mech.* 532, 269–319.
- ASTM D2488-93, 2009. Standard practice for description and identification of soils (visual-manual procedure). annual book of ASTM standard 04(08). ASTM international, West Conshohocken, PA, pp. 218–228.
- Berti, M., Simoni, A., 2005. Experimental evidence and numerical modeling of debris flow initiated by channel runoff. *Landslides* 2 (3), 171–182.
- Cannon, S.H., Gartner, J.E., Parrett, C., Parise, M., 2003. Wildfire-related debris flow generation through episodic progressive sediment bulking processes, western USA. In: Rickenmann, D., Chen, C.L. (Eds.), *Proceedings of the Third International Conference on Debris-Flow Hazards Mitigation*, pp. 71–82 (Davos, Switzerland).
- Cannon, S.H., Kirkham, R.M., Parise, M., 2001. Wildfire-related debris-flow initiation processes, Strom King Mountain, Colorado. *Geomorphology* 39 (3–4), 171–188.
- Castro, G., 1969. Liquefaction of sands. *Harvard Soil Mechanics Series* 81. Pierce Hall.
- Coe, J.A., Kinner, D.A., Jonathan, W., Godt, J.W., 2008. Initiation conditions for debris flows generated by runoff at chalk cliffs, Central Colorado. *Geomorphology* 36 (3–4), 270–297.
- Cui, P., Zhou, G.D., Zhu, X.H., Zhang, J.Q., 2013. Scale amplification of natural debris flows caused by cascading landslide dam failures. *Geomorphology* 182 (15), 173–189.
- Daouadji, A., Darve, F., Gali, A.H., Hicher, P.Y., Laouafa, F., Lignon, S., Nicot, F., Nova, R., Pinheiro, M., Prunier, F., Sibille, L., Wan, R., 2010. Diffuse failure in geomaterials: experiments, theory and modelling. *Numer. Anal. Methods Geomech.* 35 (16), 1731–1773.
- Darve, D., 1996. Liquefaction phenomenon of granular materials and constitutive stability. *Eng. Comput.* 13 (7), 5–28.
- Eckersley, J.D., 1990. Instrumented laboratory flowslides. *Géotechnique* 40 (3), 489–502.
- Eglit, M., Demidov, K.S., 2005. Mathematical modelling of snow entrainment in avalanche motion. *Cold Reg. Sci. Technol.* 43, 10–23.
- Gregoretti, C., 2000. The initiation of debris flow at high slopes: experimental results. *J. Hydraul. Res.* 38 (2), 83–88.
- Gregoretti, C., Fontana, G.D., 2008. The triggering of debris flow due to channel-bed failure in some alpine headwater basins of the dolomites: analyses of critical runoff. *Hydrol. Process.* 22 (13), 2248–2263.
- Hird, C.C., Hassona, F.A.K., 1990. Some factors affecting the liquefaction and flow of saturated sands in laboratory tests. *Eng. Geol.* 28 (1–2), 149–170.
- Hu, W., Xu, Q., Rui, C., Huang, R.Q., van Asch, T.W.J., Zhu, X., Xu, Q.Q., 2015. An instrumented flume to investigate the initiation mechanism of the postearthquake huge debris flow in the southwest of China. *Bull. Eng. Geol. Environ.* 74 (2), 393–404.
- Huang, R.Q., Li, W.L., 2009. Analysis of the geo-hazards triggered by the 12 may 2008 Wenchuan earthquake, China. *Bull. Eng. Geol. Environ.* 68 (3), 363–371.
- Ishihara, K., 1993. Liquefaction and flow failure during earthquakes. *Géotechnique* 43 (3), 349–451.
- Iverson, R.M., Reid, M.E., Logan, M., LaHusen, R.G., Godt, J.W., Griswold, J.P., 2011. Positive feedback and momentum growth during debris-flow entrainment of wet bed sediment. *Nat. Geosci.* 4, 116–121.
- Johnson, A.M., Rodine, J.R., 1984. Debris flow. In: Brundsen, D., Prior, D.B. (Eds.), *Slope Instability*. Wiley, Chichester, pp. 257–361.
- Kean, J.W., McCoy, S.W., Tucker, G.E., Staley, D.M., Coe, J.A., 2013. Run-off generated debris flow: observations and modeling of surge initiation, magnitude, and frequency. *J. Geophys. Res. Earth Surf.* 118 (4), 2190–2270.
- Kramer, L.L., Seed, H.B., 1998. Initiation of soil liquefaction under static loading conditions. *J. Geotech. Eng. ASCE* 114, 412–430.
- Lade, P.V., Liggio, C.D., Yamamoto, J.A., 1998. Effects of non-plastic fines on minimum and maximum void ratios of sand. *Geotech. Test. J.* 21 (4), 336–347.
- Larsen, I., Pederson, J.L., Schmidt, J.C., 2006. Geologic versus wildfire controls on hillslope processes and debris flow initiation in the green river canyons of dinosaur national monument. *Geomorphology* 81 (1–2), 114–127.
- McDougall, P., Hungr, O., 2005. Dynamic modelling of entrainment in rapid landslides. *Geotech. J.* 41 (12), 1084–1097.
- Olivares, L., 2001. Static liquefaction: a hypothesis for explaining transition from slide to flow in pyroclastic soils. *Proc. OSSMGE CT-11 Conf. on Transition from Slide to Flow-Mechanisms and Remedial Measure*, Trabzon, Turkey.
- Tang, C., van Asch, T.W.J., Chang, M., Chen, G.Q., Zhao, X.H., Huang, X.C., 2012. Catastrophic debris flows on 13 August 2010 in the Qingping area, southwestern China: the combined effects of a strong earthquake and subsequent rainstorms. *Geomorphology* 139–140, 559–576.
- Tang, C., Zhu, J., Li, W.L., 2009. Rainfall-triggered debris flows following the Wenchuan earthquake. *Bull. Eng. Geol. Environ.* 68 (2), 187–194.

- Tognacca, C., Bezzola, G.R., 1997. Debris-flow initiation by channel bed failure. In: Chen, C. (Ed.), *Proc. of the first Int. Conf. on Debris Flow, Hazards and Mitigation*. American Society of Civil Engineers, San Francisco, pp. 44–53.
- Tognacca, C., Bezzola, G.R., Minor, H.E., 2000. Threshold criterion for debris-flow initiation due to channel bed failure. In: Wiczorek, G.F. (Ed.), *Proceedings Second International Conference on Debris Flow Hazards Mitigation: Mechanics, Prediction and Assessment*, Taipei, pp. 89–97.
- Van Asch, T.W.J., Tang, C., Zhu, J., Alkema, D., 2014. An integrated model to assess critical rain fall thresholds for the critical run-out distances of debris flows. *Nat. Hazards* 70 (1), 299–311.
- Xu, Q., Zhang, S., Li, L., Van Asch, T.W.J., 2012. The 13 August 2010 catastrophic debris flows after the 2008 Wenchuan earthquake, China. *Nat. Hazards Earth Syst. Sci.* 12 (1), 201–216.